Optimal Eco-Driving Control of Connected and Autonomous Vehicles Through Signalized Intersections

Chao Sun, *Member, IEEE*, Jacopo Guanetti, *Member, IEEE*, Francesco Borrelli, *Fellow, IEEE*, and Scott J. Moura, *Member, IEEE*

***Abstract*—This article focuses on the speed planning problem for connected and automated vehicles (CAVs) communicating to traffic lights. The uncertainty of traffic signal timing for signalized intersections on the road is considered. The eco-driving problem is formulated as a data-driven chance-constrained robust optimization problem. Effective red-light duration (ERD) is defined as a random variable, and describes the feasible passing time through the signalized intersections. Usually, the true probability distribution for ERD is unknown. Consequently, a data-driven approach is adopted to formulate chance constraints based on empirical sample data. This incorporates robustness into the eco-driving control problem with respect to uncertain signal timing. Dynamic programming (DP) is employed to solve the optimization problem. The simulation results demonstrate that the proposed method can generate optimal speed reference trajectories with 40% less vehicle fuel consumption, while maintaining the arrival time at a similar level compared to a modified intelligent driver model (IDM). The proposed control approach significantly improves the controller's robustness in the face of uncertain signal timing, without requiring to know the distribution of the random variable *a priori*.**

***Index Terms*—Connected and automated vehicle (CAV), data-driven, eco-driving, robust control, traffic signal.**

I. Introduction

CONNECTED and automated vehicle (CAV) technology is revolutionizing the automotive industry. In particular, CAVs may significantly improve safety, energy economy, and convenience, with the abilities for self-driving, path/velocity planning, vehicle-to-infrastructure (V2I), and vehicle-to-vehicle (V2V) communications [1], [2]. Optimal eco-driving control—a promising technology enabled by CAVs—is defined as a velocity planning and control method to achieve better energy economy [3]. Intuitively speaking, optimal eco-driving seeks the best velocity trajectory to minimize energy consumption.

Manuscript received July 20, 2019; revised November 12, 2019; accepted January 9, 2020. Date of publication January 21, 2020; date of current version May 12, 2020. This work was supported in part by the Advanced Research Projects Agency-Energy, U.S. Department of Energy under Award DE-AR0000791; and in part by the Natural Science Foundation of China under Grant U1964206 and Grant 51705019. *(Corresponding author: Chao Sun.)*

Chao Sun is with the Department of Mechanical and Automotive Engineering, Beijing Institute of Technology, Beijing 100081, China (e-mail: chaosun@bit.edu.cn).

Jacopo Guanetti and Francesco Borrelli are with the Department of Mechanical Engineering, University of California at Berkeley, Berkeley, CA 94704 USA (e-mail: jacopoguanetti@berkeley.edu; fborrelli@berkeley.edu).

Scott J. Moura is with the Department of Civil and Environmental Engineering, University of California at Berkeley, Berkeley, CA 94704 USA (e-mail: smoura@berkeley.edu).

Digital Object Identifier 10.1109/JIOT.2020.2968120

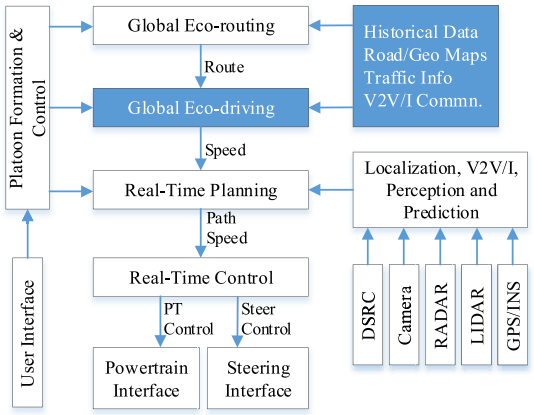

Fig. 1. Hierarchical control architecture for energy-optimal operation of CAVs. Generally, 100% safety and energy efficiency can be achieved by combining eco-driving with real-time planning/control. This article focuses on the global eco-driving control problem facing traffic light disturbances.

A. Overall Control Architecture

In literature, optimal eco-driving is also referred as ecological driving, speed trajectory planning, driving advisory, or driver-assistance systems [4]. One may conceptualize eco-driving as one supervisory layer within a multilayer hierarchical control architecture for CAVs, depicted in Fig. 1. Due to space limitation, this architecture cannot be comprehensive, but it covers the critical blocks required for CAV implementation.

1) The eco-routing block determines the most energy-efficient route, given user requirements and route data (such as road grade, traffic condition, or facilities [5]). This block outputs the optimal route, i.e., a set of waypoints along with the intersection locations, speed limits, and road grade [6]. Note that eco-routing and eco-driving can be coupled together and work simultaneously.
2) The eco-driving block is the scope of this article. This block takes route information and computes the energy-optimal speed trajectory. Some constraints depend on

the driving context: for instance, passing a signalized intersection green phases. Historical data of signal phase and timing (SPaT) and dedicated short-range communications (DSRC) might be required.

Generally, eco-routing and eco-driving do not have hard real-time requirements, and can be implemented in the cloud. Conversely, the blocks described next are safety critical, and need to be executed in real time on the vehicle.

1) The real-time planning block solves several planning problems for CAVs, which may include maneuver planning (e.g., decision to stay in a lane or change), path planning, and trajectory planning. These blocks also depend on the driving context, and their boundaries are quite blurred [7].
2) The real-time control block tracks the longitudinal and lateral trajectories, and interfaces with the vehicle actuators. A CAV control architecture may be interfaced to the vehicle powertrain (e.g., controlling engine torque, braking torque, and gear shifting) and to its steering system.

The real-time planning and control blocks require feedback from the vehicle, its position relative to the surrounding environment, and predictions of moving obstacles [8]. A CAV may be equipped with a GPS/INS unit for localization, cameras, radars, and lidars for perception, and DSRC units for communication [9]. These data are processed by the localization and perception block, which estimates the position of the ego CAV and its surroundings. This CAV control architecture can be generalized to a network system by the platoon formation and control block.

B. Disturbance Analysis and Scope Clarification

The speed planning or control problem of a CAV faces a lot of uncertain disturbances or potential factors that would affect its performances.

1) Traffic lights at intersections can be divided into two types: fixed and actuated. Traffic lights enforce a series of time-varying constraints in eco-driving.
2) Surrounding vehicles and car waiting queue affect the speed control performance. Especially, the car waiting queue can be estimated via high-resolution traffic data or floating car data [10], [11].
3) Pedestrians at crossings, especially where there is no traffic light, demonstrate very strong stochasticity.
4) Lane-changing behaviors, which are affected by the environment and driving intentions, require fast dynamics control of the vehicle.
5) Accidents, road work, or congestions are another type of uncertain disturbances that would influence the eco-driving performances.

In CAV eco-driving, each of the above disturbances may require different perception, communication, and control methods to ensure robust operation. In particular, combining eco-driving with a real-time control layer introduced in Fig. 1 is extremely important to ensure 100% safety and is more realistic. This is our next step study.

Due to limited space, we are not able to discuss all the above disturbances. This article focuses on the eco-driving problem regarding traffic light disturbances. Over the past five years, the optimal eco-driving problem has been intensively studied [12], [13], which can be classified into two groups: with or without traffic lights considered.

C. Literature Review

When traffic light is not considered, the eco-driving control scenario is simpler. Dynamic programming (DP)-based approach is found in [14] for the speed control of an internal combustion engine (ICE) vehicle to obtain the optimal velocity profile. DP is further applied to an electric vehicle (EV) in [15] for eco-driving control. Both of them have demonstrated that properly designed speed profile is able to significantly improve the vehicle energy efficiency. More comprehensively, a cloud-based velocity profile optimization approach is designed in [16] under a spatial domain formulation. Spatial optimization is further adopted by [17] for ecological driving, with a short-term adaptation level added to avoid traffic congestion. Optimal eco-driving has also been integrated to the energy management of hybrid EVs, with Pontryagin's minimal principle used to solve the optimization problem in [18]. From existing studies, heuristic- or optimization-based strategies have been successfully utilized to gain better fuel efficiency in eco-driving without the SPaT information used [19], [20].

When traffic light is considered, the SPaT information is critical [21], [22]. Extra constraints are required when an intersection is controlled by traffic signals [23]. In [24] and [25], traffic lights location, SPaT are taken into account. Optimization is conducted to find the optimal driving pace by enforcing that the vehicle only drives through green-light windows. DP is combined with a pruning algorithm to reduce the optimization domain [26]. By considering each signalized intersection as one stage, a multistage pseudospectral control method is proposed in [27] in an arterial road structure. Hierarchical MPC is adopted in [28], and demonstrated effective online eco-driving control capabilities. Yang *et al.* [29] considered the car waiting queue in a multilane road scenario, and designed an eco-cooperative adaptive cruise control scheme. Assuming the engine operates only on the optimal brake specific fuel consumption (BSFC) line, sequential convex optimization is applied in [30] for eco-driving through multiple signalized intersections.

In the aforementioned eco-driving studies, the SPaT information is assumed to be deterministic and known. However, this assumption does not match well the reality. Uncertainty always exists due to varying patterns of traffic lights as depicted in Fig. 2. In reality, the actual SPaT information distributions at different intersections are difficult to obtain. In [31], SPaT was predicted based on the current phase and averaged timing data, and further used in velocity planning. Differently, we follow the approach in [32] and propose a robust control approach using the probability distribution of SPaT, which could be more flexible and requires less information. The issue of SPaT uncertainty in optimal

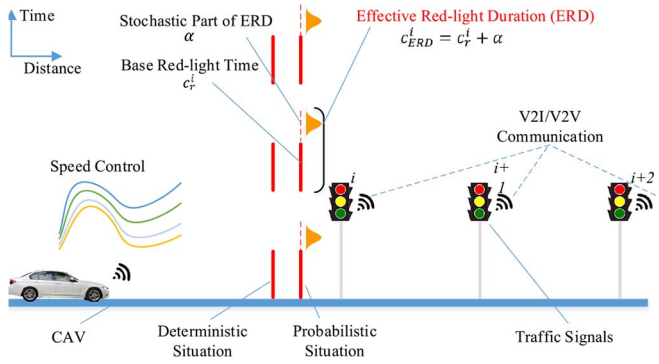

Fig. 2. Optimal eco-driving of CAV through multiple traffic signals, where vehicle speed control is the main task. ERD represents the infeasible passing time at an intersection.

eco-driving is significant, yet not fully addressed in the existing literature. We intend to solve this problem by introducing a data-driven chance constraint in eco-driving control.

D. Main Contributions

In this article, we investigate a data-driven chance-constrained eco-driving approach which is robust to uncertain feasible vehicle passing times, with the goal to simultaneously achieve energy economy and safety. The feasible passing time of a vehicle through an uncertain signalized intersection is formulated in terms of the effective red-light duration (ERD), illustrated in Fig. 2. The main contributions of this article include the following.

1) Robust control formulation of CAV eco-driving through multiple signalized intersections with uncertain SPaT is systematically presented.
2) A distributionally robust chance-constrained approach is developed to solve the robust optimal eco-driving control problem, demonstrating that the vehicle fuel consumption can be significantly reduced by sacrificing less than 5% of the arrival time.
3) A data-driven equivalent reformulation of the distributionally robust chance constraint (DCC) is given, without knowing the distribution of random variable *a priori* [33].

The remainder of this article is organized as follows. Section II describes the vehicle and traffic signal model. Section III introduces the robust optimal eco-driving control strategy in a spatial formulation that considers uncertain feasible passing time at signalized intersections. Section IV details a data-driven equivalent reformulation of the distributionally robust chance-constrained program. Section V presents the main results, and Section VI summarizes the contributions. Though an ICE vehicle is studied in this article, our proposed approach can easily adapt to electrified or hybrid vehicles. The method is independent of the vehicle powertrain.

II. Vehicle and Traffic Signal Modeling

This section details the vehicle and traffic signal mathematical models used for eco-driving speed trajectory optimization.

A. Vehicle Dynamics

The subject vehicle is equipped with a gasoline ICE and a 6-speed gearbox. Since speed planning is the main task in optimal eco-driving control, we consider longitudinal vehicle dynamics and disregard the lateral dynamics [34]. The longitudinal acceleration is calculated by

$$ma = \frac{r_{gb}T_{\text{eng}} - T_{\text{brk}}}{R_{\text{whl}}} - mg(\cos(\theta)C_r - \sin(\theta)) - \frac{1}{2}\rho A C_d v^2 \tag{1}$$

$$C_r = C_{r1} + C_{r2}v \tag{2}$$

where m is the vehicle mass, a is the acceleration, r_{gb} is the product of the gearbox and final drive ratios, T_{eng} is the ICE output torque, R_{whl} is the wheel rolling radius, g is the gravitational acceleration, θ is the road grade, and C_r is the rolling resistance coefficient. Parameters ρ, A, and C_d are the air density, frontal area, and air drag coefficient, respectively. Variable v is the vehicle velocity, T_{brk} is the braking torque enforced on the wheels, and C_{r1} and C_{r2} are rolling resistance constants. The longitudinal velocity is computed by

$$v = \frac{\omega_{\text{eng}}}{r_{\text{gb}}} \tag{3}$$

where ω_{eng} is the ICE rotation speed. The ICE fuel consumption is modeled as a static nonlinear map $\psi(\cdot,\cdot)$ of the engine torque and speed

$$\dot{m}_{\text{fuel}} = \psi\left(T_{\text{eng}}, \omega_{\text{eng}}\right) \tag{4}$$

where $\dot{m}_{\text{fuel}}$ is the instantaneous fuel consumption, and ψ is the prestored fuel map (e.g., a look-up table). The transmission efficiency is ignored in this article. Assume r_{fd} is the final drive ratio. The integrated transmission ratio is formulated as a function of the gear number N_{gb}

$$r_{\text{gb}} = f\left(N_{\text{gb}}\right) \cdot r_{\text{fd}}, \qquad N_{\text{gb}} \in \{1,2,3,4,5,6\}. \tag{5}$$

B. Fixed Traffic Signal Timing

Traffic signals are space indexed and time varying in the optimal eco-driving problem. Assume the total length of the target driving route is s_f. The position of the ith traffic signal is denoted by s^i. Therefore

$$s^i \in \left[0, s_f\right], \quad i = \{1,2,3,4,5\cdots I\} \tag{6}$$

where I is the total number of traffic signals along the route.

In our formulation, each traffic signal has an independent periodic clock. We denote the absolute time as $t \in R^+$, and the clock period at intersection i as $c_f^i \in R^+$. Clock time zero denotes the beginning of the red-light phase. Every intersection can have a different clock period. The red-light duration is denoted by c_r^i

$$c_r^i \in \left[0, c_f^i\right]. \tag{7}$$

Denote by c_0^i the clock time when the vehicle departs from its origin, and by i the traffic light index number. Suppose t_p^i is the time at which the subject vehicle passes through the

ith intersection in the traveling time domain. We can compute the corresponding time in the periodic traffic signal clock timing by

$$c_p^i = \left(c_0^i + t_p^i\right) \bmod c_f^i \tag{8}$$

where c_p^i is the vehicle passing time in the signal-cycling clock. The modulo operator allows for conversion from the traveling time domain to the periodic traffic signal clock time domain. Definitions of the symbols are illustrated in Fig. 3.

In the case of unsignalized intersections or crossings, the criticality of motion planning and dynamics control would increase. Also, they would necessarily rely on the onboard perception sensors (camera, radar, and lidar) to assess the passing conditions in real time—a topic not discussed in this article.

C. Uncertain Traffic Signal Timing

In the fixed signal timing setting, the SPaT [i.e., c_r^i in (15)] is assumed to be deterministic and perfectly known by the vehicle. However, as illustrated in Fig. 2, the feasible passing time at a signalized intersection is usually uncertain and random. In this article, ERD is defined to describe the feasible passing time, denoted as c_{ERD}^i

$$c_{\text{ERD}}^i = c_r^i + \alpha^i. \tag{9}$$

Parameter c_r^i is the base or nominal red-light duration. The random variable α^i is a comprehensive stochastic time delay at the ith intersection, caused by traffic signal variation, vehicle waiting queue, or other factors. Assume α^i is distributed over the green-light duration, so that $\alpha^i \in [0, (c_f^i - c_r^i)]$. Note that the probability distribution function of α^i is obtained via real data (see Section V-C).

From the real traffic SPaT data collected in [35], it can be seen that the total signal cycling period is not affected by these uncertain factors, meaning c_f^i is fixed. Therefore, in this article, we assume c_f^i is deterministic and known for all the intersections.

III. Robust Optimal Eco-Driving

Next, we formulate and solve the robust optimal eco-driving control problem under uncertain signal timing.

A. Problem Formulation

The optimal eco-driving control problem is formulated as a nonlinear spatial trajectory optimization problem which seeks to minimize the vehicle's total fuel consumption and final arrival time. The cost functional J is defined as

$$\begin{aligned} J &= \int_0^{s_f} \left(\lambda \left|\frac{\dot{m}_{\text{fuel}}(s)}{v(s)}\right| + (1-\lambda)\left|\frac{d}{ds}t(s)\right|\right) ds \\ &= \lambda \cdot |m_{\text{fuel}}(s_f)| + (1-\lambda)\cdot |t(s_f)| \end{aligned} \tag{10}$$

where λ is a tuning weight, s is traveled distance, $|m_{\text{fuel}}(s_f)|$ is normalized cumulative fuel consumption, and $|t(s_f)|$ is normalized arrival time at destination. Thus, the units of fuel consumption cost and arrival time cost are consistent. Engine torque, wheel braking torque, and transmission gear number are chosen as the control variables

$$u = \left[T_{\text{eng}}(s), T_{\text{brk}}(s), N_{\text{gb}}(s)\right]^T. \tag{11}$$

The vehicle velocity and travel time are chosen as the state variables

$$x = [v(s), t(s)]^T \tag{12}$$

$$\frac{dv}{ds}(s) = \frac{a(s)}{v(s)}, \qquad \frac{dt}{ds}(s) = \frac{1}{v(s)}. \tag{13}$$

Here, we restrict $v(s) > 0$. The vehicle stops are modeled by assuming $v(s)$ a small positive constant.

The optimization problem is subject to the vehicle dynamics introduced in (1)–(5), traffic light dynamics from (6)–(8), and the following constraints:

$$T_{\text{eng}}^{\min} \le T_{\text{eng}}(s) \le T_{\text{eng}}^{\max} \quad \forall\, s \in [0, s_f] \tag{14a}$$

$$T_{\text{brk}}^{\min} \le T_{\text{brk}}(s) \le T_{\text{brk}}^{\max} \quad \forall\, s \in [0, s_f] \tag{14b}$$

$$N_{\text{gb}}(s) \in \{1, 2, 3, 4, 5, 6\} \quad \forall\, s \in [0, s_f] \tag{14c}$$

$$v(0) = v(s_f) = v^{\min}(s) \tag{14d}$$

$$a^{\min} \le a(s) \le a^{\max} \quad \forall\, s \in [0, s_f] \tag{14e}$$

$$v^{\min}(s) \le v(s) \le v^{\max}(s) \quad \forall\, s \in [0, s_f] \tag{14f}$$

$$t(s_f) \le t_f. \tag{14g}$$

A key beneficial feature of a spatial trajectory formulation (as opposed to temporal) is that the final destination arrival times do not need to be known *a priori* in the global optimization approach. A preset maximal arrival time constraint t_f is imposed on the final state variable $t(s_f)$, to balance fuel economy and travel time.

Based on the level of knowledge on the traffic signal timing, three situations are discussed and formulated: 1) traffic signal timing is deterministic and known; 2) signal timing is random but the probability distribution is known; and 3) signal timing is random and the probability distribution is unknown.

1) Problem 1 (Deterministic Timing): For deterministic traffic signal timing, c_r^i is deterministic and known. The following constraint ensures the vehicle passes through signalized intersections during the green phase:

$$c_p^i \ge c_r^i. \tag{15}$$

The optimal eco-driving formulation of (10)–(14) with constraint (15) is denoted as Problem 1. Constraint (15) gives the controller the biggest flexibility of speed planning, while respects traffic rules at the same time.

2) Problem 2 (Random Timing With Known Probability Distribution): Using the definition of ERD in (9), the traffic signal passing constraint in (15) is modified to

$$c_p^i \ge c_{\text{ERD}}^i = c_r^i + \alpha^i \qquad \forall\, \alpha^i \in \left[0, \left(c_f^i - c_r^i\right)\right]. \tag{16}$$

However, enforcing the constraint above for all values in the support of α^i may be too restrictive. For example, if there exists a small but nonzero probability of $\alpha^i = (c_f^i - c_r^i)$ during heavy congestions, then all feasible solutions will require the vehicle to wait a whole signal cycle before proceeding through the intersection. This is not reasonable.

Instead, traffic signal passing can be enforced up to a certain probability. Mathematically, this amounts to enforcing a chance constraint

$$\Pr\left(c_p^i \geq c_r^i + \alpha^i\right) \geq 1 - \eta \quad \forall\ \eta \in\ [0, 1] \tag{17}$$

where η is the risk level of running red lights. This is typically taken as a small number, such as 0.01 or 0.001. Let $F(\alpha^i)$ indicate the cumulative distribution function (CDF) of α^i. Equation (17) can be rewritten as

$$\Pr\left(\alpha^i \leq c_p^i - c_r^i\right) = F\left(c_p^i - c_r^i\right) \geq 1 - \eta \quad \forall\ \eta \in\ [0, 1]. \tag{18}$$

We assume the CDF $F(\cdot)$ is bijective, and therefore has an inverse function $F^{-1}(\cdot)$. Thus, we can solve for the optimization variable c_p^i to obtain

$$c_p^i \geq c_r^i + F^{-1}(1 - \eta) \quad \forall\ \eta \in\ [0, 1]. \tag{19}$$

Again, c_p^i is the passing time of the subject vehicle through the ith intersection in the signal-cycling clock, which is a function of the control and state variables, $c_p^i(x, u)$. After replacing constraint (15) with (19), we arrive at the robust optimal eco-driving control formulation. This formulation is denoted as Problem 2, which requires the CDF of α^i to be known to solve the problem.

3) Problem 3 (Random Timing With Unknown Probability Distribution): Assume α^i is a random variable over time 0 to $(c_f^i - c_r^i)$, whose probability distribution is usually unknown in real life. The distribution of α^i might also vary at different times of the day (rush hour versus 3:00 A.M.), seasons, or locations. Thus, α^i may not be accurately modeled by a single probability distribution function.

The optimal eco-driving formulation of (10)–(14) with unknown distribution of α^i is denoted as Problem 3, which we intend to solve via the data-driven chance-constrained optimal control in Section IV.

4) Problem 4 (Random Timing With Unknown Probability Distribution and Estimated Car Waiting Queue): Car waiting queue impacts the velocity optimization problem by causing greater delay on the feasible traveling time window while the vehicle is driving through intersections. In this article, we assume that the queue length s_w^i and caused delay t_w^i are estimated via high-resolution traffic data, as illustrated in Fig. 3. Thus, we can have

$$c_p^i \geq c_r^i + t_w^i + F^{-1}(1 - \eta) \quad \forall\ \eta \in\ [0, 1]. \tag{20}$$

This formulation while considering the car waiting queue is denoted as Problem 4, which can also be solved via the proposed data-driven chance-constrained optimal control approach.

B. Dynamic Programming

DP is employed to solve the nonlinear optimal control problems 1 and 2, with an implementation methodology described in [36]. By breaking a complicated problem into simpler subproblems in a recursive manner, DP is able to solve multistage optimal decision-making problems.

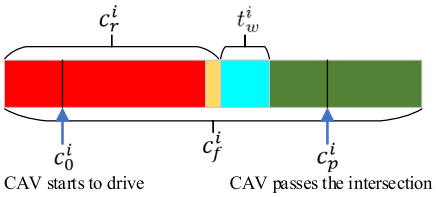

Fig. 3. Definitions of the symbols used to describe the SPaT at an intersection.

Denoting the cost at the kth step by $g_k(x_k, u_k)$, the cost function (10) can be approximated by a discrete summation

$$J = \sum_{k=0}^{N-1} g_k(x_k, u_k) + g_N(x_N). \tag{21}$$

According to Bellman's principle of optimality equation, the objective is to minimize the following cost-to-go function at each stage k:

$$\begin{aligned} V_k(x_k) &= \min\{g_k(x_k, u_k) + V_{k+1}(x_{k+1})\} \\ &= \min\{g_k(x_k, u_k) + V_{k+1}(f(x_k, u_k))\} \end{aligned} \tag{22}$$

where $V_k(x_k)$ is the value function (also known as "cost-to-go" function). It represents the minimum cost from stage k to stage N, given that the state is initialized to x_k at stage k. Note, also, that substitution of general dynamics $x_{k+1} = f(x_k, u_k)$. The terminal cost at $k = N$ is given by the boundary (also known as terminal) conditions in (14)

$$V_N(x_N) = g_N(x_N). \tag{23}$$

Assume the optimal control and state variable trajectories for the optimal control problem are U^* and X^*, respectively, then

$$\begin{aligned} U^* &= \left[u_0^*, u_1^*, u_2^*, \ldots, u_{N-1}^*\right]^T \\ X^* &= \left[x_0^*, x_1^*, x_2^*, \ldots, x_N^*\right]^T. \end{aligned} \tag{24}$$

Based on terminal condition (23), the optimal control policy can be computed by the following backward recursive algorithm starting from step $(N - 1)$ to 0:

$$\begin{aligned} u_k^* = \arg\min_{u_k \in \mathcal{U}_D} &\{g_k(x_k, u_k) + V_{k+1}(f(x_k, u_k))\} \\ &\forall x_k \in \mathcal{X}_D \end{aligned} \tag{25}$$

where $\mathcal{U}_D$ and $\mathcal{X}_D$ are the feasible control and state variable constraint sets, respectively. Function $f(x, u)$ represents the eco-driving control system dynamics. Interested readers are referred to [37] and [38] for a detailed exposition of DP.

IV. Data-Driven Chance Constraints

When the probability distribution of α^i is unknown, a data-driven approach is employed to establish equivalent DCCs for Problems 3 and 4.

A. Distributionally Robust Chance Constraints

The optimal eco-driving control solutions could be very sensitive to ambiguous variations of the probability distribution for α^i. As such, the solutions may be suboptimal in practice with improperly formulated chance constraints. In this case, an optimization program with DCCs is proposed, where the constraint in (18) is reformulated into

$$\inf_{\mathbb{P}\in\mathcal{D}} \mathbb{P}\left\{\alpha^i \le c_p^i - c_r^i\right\} \ge 1-\eta \quad \forall\ \eta \in\ [0,1] \tag{26}$$

where $\mathbb{P}$ represents the cumulative probability distribution, and $\mathcal{D}$ is a confidence set of possible probability distributions constructed based on the distributional information. Index i indicates the intersection number, and is omitted in the following equations to simplify notation.

Normally, $\mathcal{D}$ can be easily constructed based on the moment information or other structural properties of the distribution, such as unimodality, symmetry, or convexity. However, in practice, distributional information is usually obtained from historical data, empirical experience, or prior knowledge. This is especially true for the stochastic delay α for traffic signal timing. A data-driven chance-constrained approach is adopted from [33] to find an equivalent reformulation of the DCC in (26) based on historical sample data, without any requirement on the distribution properties of α.

We use ϕ-divergence to model the distance between two probability density functions. ϕ-divergence distance D_ϕ is defined as

$$D_\phi\left(f^*\middle\|\hat{f}\right) = \int_\Omega \phi\left(\frac{f^*(\alpha)}{\hat{f}(\alpha)}\right)\hat{f}(\alpha)d\alpha \tag{27}$$

where f^* is the true, but usually unknown, probability density function, $\hat{f}$ is the probability density function estimated from sampled or empirical data, and α is the random variable. We assume ϕ to be a convex function defined on $\mathbb{R}^+$, such that $\phi(1)=0$. Examples include the Kullback–Leibler divergence ϕ_{KL}, the variance distance divergence ϕ_{VD}, and the χ divergence of order 2 ϕ_{χ^2}

$$\begin{aligned}
\phi_{\mathrm{KL}}(x) &= x\log x - x + 1 \quad && \forall\ x \in\ [0,+\infty)\\
\phi_{\mathrm{VD}}(x) &= |x-1| && \forall\ x \in\ [0,+\infty)\\
\phi_{\chi^2}(x) &= (x-1)^2 && \forall\ x \in\ [0,+\infty).
\end{aligned} \tag{28}$$

To ensure convexity, all the ϕ-divergence functions above are extended by

$$\phi(x) = +\infty \quad \forall\ x \in\ (-\infty, 0). \tag{29}$$

Based on the ϕ-divergence distance metric, we refine constraint (26) by constructing a confidence set of $\mathcal{D}_\phi$ as

$$\mathcal{D}_\phi = \left\{\mathbb{P}\in\mathcal{P} : D_\phi\left(f^*\middle\|\hat{f}\right) \le d, f = \frac{d\mathbb{P}}{d\alpha}\right\} \tag{30}$$

where $\mathcal{P}$ represents the set of all probability distributions that $\mathbb{P}$ could be. Scalar $d\in\mathbb{R}$ is the allowed distance between the estimated and true distributions, and can be used to tune the risk-aversion level. For a given choice of the ϕ-divergence function and d, the DCC developed in (26) can be converted into

$$\inf_{D_\phi\left(f^*\middle\|\hat{f}\right)\le d} \mathbb{P}\left\{\alpha \le c_p^i - c_r^i\right\} \ge 1-\eta \quad \forall\ \eta \in\ [0,1]. \tag{31}$$

B. Data-Based Equivalent Reformulation

In Problem 3, the true probability density function f^* in (31) is unknown. However, if empirical data on α is available, then an equivalent reformulation of this DCC can be derived, as proposed and proved by [33]. This equivalent reformulation is adopted in this article.

Here, let $\hat{\mathbb{P}}$ represent the approximated cumulative probability distribution of $\hat{f}$ estimated from empirical data, then (31) is equivalent to

$$\hat{\mathbb{P}}\left\{\alpha \le c_p^i - c_r^i\right\} \ge 1-\eta'_+ \tag{32}$$

where $\eta'_+ = \max\{\eta', 0\}$, and η' is estimated from the original risk level and ϕ-divergence distance. The formulation of η' is given in the Appendix.

Equations (32) and (42)–(44) comprise the equivalent reformulation of the DCC from (31). For a detailed proof, please refer to [33, Sec. 3]. Solving the two-variable nonlinear optimization problem in the reformulated DCC of (32) forms an alternative way to realize robust control.

The perturbed risk level η' for KL divergence, VD divergence, and χ^2 divergence are given below for implementation purposes, denoted as η'_{KL}, η'_{VD}, and η'_{χ^2}, respectively. Assume that the original risk level η is a small number, therefore

$$\eta'_{\mathrm{VD}} = \eta - \frac{d}{2} \tag{33}$$

$$\eta'_{\chi^2} = \eta - \frac{\sqrt{d^2 + 4d\left(\eta-\eta^2\right)} - (1-2\eta)d}{2d+2}. \tag{34}$$

For the KL divergence, the perturbed risk level is

$$\eta'_{\mathrm{KL}} = 1 - \inf_{x\in(0,1)}\left\{\frac{e^{-d}x^{1-\eta}-1}{x-1}\right\} \tag{35}$$

which can be computed by bisection line search.

C. Implementation Procedure

The workflow to establish an equivalent reformulation of the DCC based on collected empirical data is summarized in Fig. 4. The chance reliability η and ϕ-divergence distance d are set at the design stage by the control engineer.

The approximated cumulative probability function $\hat{\mathbb{P}}$ and the density function $\hat{f}$ are computed from an empirical database. The perturbed risk level η' can be found via bisection line searching once the chance reliability η and the ϕ-divergence distance d have been selected.

The equivalent reformulated DCC can be obtained by following the procedure in Fig. 4. Appending this reformulated DCC to Problem 3 yields an optimization program for the optimal eco-driving problem with random α with unknown probability distribution. The only requirement is access to empirical or historical data on α.

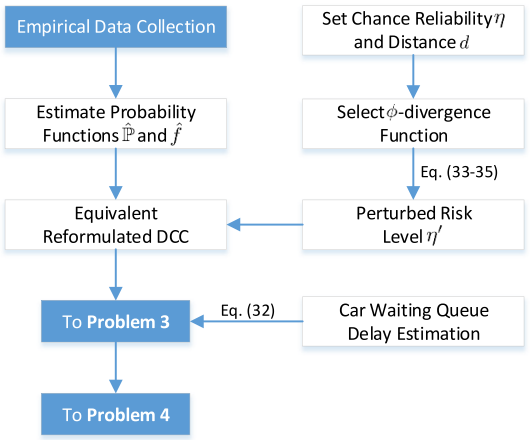

Fig. 4. Workflow to construct an equivalent formulation of the DCC based on empirical or historical data.

D. Parameter Selection

With the reformulated DCC, we can calculate the inverse function of $F^{-1}(1-\eta'_+)$ in (32) without knowing any structural properties of the random variable distribution. Several questions could be asked with respect to the practical implementation of this approach.

1) What is the proper size of the historical sample data N_s for the random variable α?
2) How to choose the distance between the estimated and true distribution d, using the ϕ-divergence criterion?
3) What is the relationship between N_s and d?

Intuitively, the three questions above are closely related to each other. The distance d can decrease toward 0 as the sample data size N_s tends to infinity. Due to limited data, however, d is always selected to be greater than 0 to ensure conservatism. The dimension of the random variable is also critical in deciding a proper size for N_s.

A simulation experiment is conducted in this section to test the performance of the reformulated DCC, and numerically answer the above questions. Here, we assume that α is a truncated Gaussian random variable, whose true probability distribution is unknown to the control engineer

$$\alpha \sim \mathcal{N}_{[0,30]}(6, 16) \in [0, 30]. \tag{36}$$

We set the chance reliability parameter $\eta = 0.03$. The value of inverse function $F^{-1}(1-\eta)$ with true distribution (36) is calculated as a benchmark. According to the reformulated equivalent DCC, an alternative inverse function $F^{-1}(1-\eta'_+)$ is used to replace $F^{-1}(1-\eta)$. Given randomly generated sample data with size N_s and a predefined distance d, inverse function $F^{-1}(\cdot)$ can be calculated. The results are demonstrated in Fig. 5.

As can be seen, when $d = 0.00001$ and 0.0001, the alternative estimates F^{-1} gradually converge to the true value as N_s grows. When the sample data size N_s is greater than 500, the marginal improvement is trivial. As d increases to 0.001, the χ^2 and KL divergence estimates of F^{-1} exceed the true value when N_s is greater than 200, indicating that $F^{-1}(1-\eta'_+)$ tends to be more conservative when d is relatively larger. This

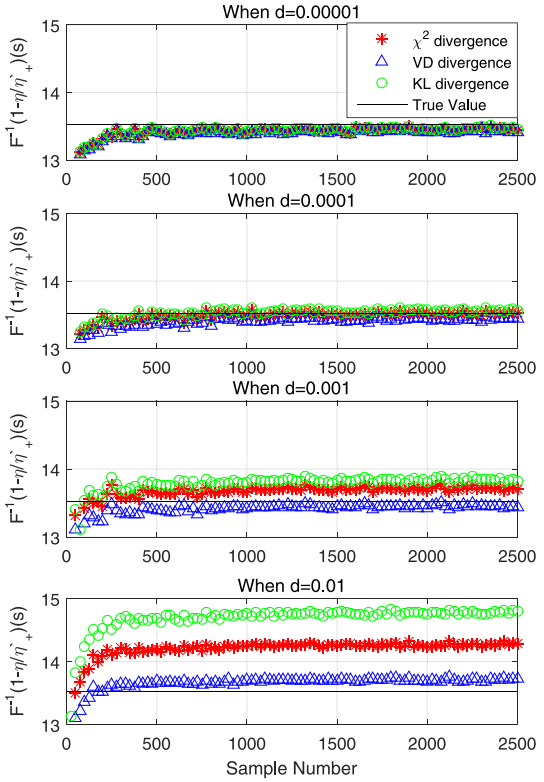

Fig. 5. Inverse function $F^{-1}(\cdot)$ results with different sample data sizes N_s. Four values for distance d are selected, which are 0.00001, 0.0001, 0.001, and 0.01, respectively.

phenomenon is further illustrated in the $d = 0.01$ case. Here, KL, χ^2, and VD divergence F^{-1} converge to nearly 14.8, 14.3, and 13.7, respectively. These results are all greater than the true value of 13.5. Moreover, we can see that when the sample data size is small (below 200 for example), then F^{-1} converges faster to the true value with greater values of d.

Based on the above numerical simulation results and the definition of d, we formulate d as a function of the sample data size density (N_s/R_α), where R_α is the dimension of the sample data

$$d = f\left(\frac{N_s}{R_\alpha}\right) = a_1 e^{b_1 \frac{N_s}{R_\alpha}} + a_2 e^{b_2 \frac{N_s}{R_\alpha}} + c \tag{37}$$

where a_1, b_1, a_2, b_2, and c are coefficients that can be fit via regression methods based on sample data. The first term in (37) is used to control the convergence trend, and the second term is used to control the decay rate. The regression model (37) partially answers the three questions above regarding parameter selection in the equivalent DCC. Still, proper selection of these parameters requires decision makers to have adequate empirical knowledge of the random variable.

V. Simulations

Three eco-driving control approaches under different traffic signal scenarios are simulated in this section. The three approaches include: 1) deterministic control via Problem 1; 2) robust control via Problem 2; and 3) data-driven chance-constrained robust control via Problems 3 and 4. Note that we

TABLE I
SUBJECT VEHICLE PARAMETERS

Parameter (Unit)	Value	Parameter (Unit)	Value
m (kg)	1745	r_{fd}	3.51
R_{whl} (m)	0.3413	$\omega_{\text{eng}}^{\max}$ (rad/s)	600
A (m^2)	2.841	$T_{\text{eng}}^{\max}$ (Nm)	240
ρ (kg/m^3)	1.1985	gearbox ratios	4.584, 2.964,
C_d	0.356		1.912, 1.446,
C_r	0.0084, 1.2e-4		1, 0.74

TABLE II
POSITION AND SPAT INFORMATION OF SAMPLE ROUTES

	Route 1			Route 2			1&2	
No.	Type	D^i (m)	c_0^i*	Type	D^i (m)	c_0^i*	c_f^i	c_r^i
1	signal	200	10	signal	200	0	60	30
2	signal	400	30	signal	400	20	60	30
3	signal	600	0	signal	600	0	60	30
4	stop	800	–	signal	800	20	60	30
5				signal	1000	0	60	30
6				signal	1200	25	60	30
7				signal	1400	10	60	30
8				stop	1600	–	60	30

* Arbitrarily selected values.

assume all traffic light SPaT information is obtained from the Cloud in real time.

A. Setup and Baseline Model

1) Vehicle and Route Parameters: The vehicle parameters and engine fuel map used for simulation are extracted from Autonomie [39], and summarized in Table I. The maximum and minimal velocity limits are set to 16 and 0 m/s, respectively.

Two sample driving routes with 3 and 7 signalized intersections are considered, and named as route 1 and route 2, respectively. All of the full cycling periods c_f^i and red-light durations c_r^i are set to 60 and 30 s, respectively. The beginning time c_0^i is arbitrarily selected between 0 and 30 s. Other realistic selections of the full cycling time and red-light duration can also be incorporated in the proposed optimal eco-driving control strategy. The position and timing information for the two sample routes are summarized in Table II.

2) Modified Intelligent Driver Model: A modified intelligent driver model (IDM) is introduced as a baseline model for comparison purposes. The basic IDM is based on the computation of the desired distance between the eco-vehicle and the front vehicle [40]. When there is no preceding vehicle, the road speed limit is used as a velocity reference.

Assuming that the desired distance between the subject vehicle and front vehicle is D_{des}, then

$$D_{\text{des}} = D_{\text{des}}^{\min} + v \cdot t_{\text{hw}} - \frac{vD_{\text{sf}}}{2\sqrt{a^{\max}a_c}} \tag{38}$$

where $D_{\text{des}}^{\min}$ is the minimal vehicle distance, t_{hw} is the desired time headway to the preceding vehicle, D_{sf} is the real distance between the subject vehicle and preceding vehicle, $a^{\max}$ is the maximal vehicle acceleration ability, and a_c is the preferred deceleration for comfort.

The vehicle acceleration at each time step is computed by comparing the desired gap distance with the current distance. An additional speed limit term is added to ensure safety

$$a = a^{\max}\left[1 - \left(\frac{v}{v^{\max}}\right)^4 - \left(\frac{D_{\text{des}}}{D_{\text{sf}}}\right)^2\right]. \tag{39}$$

To interact with traffic signals or stop signs, we modified the IDM by enabling the driver model to preview the traffic signal status at a human-vision distance D_v. Assuming that the current location of the vehicle is s, the driver model in (39) becomes

$$a = \begin{cases} a^{\max}\left[1 - \left(\frac{v}{v^{\max}}\right)^4 - \left(\frac{D_{\text{des}}}{D_{\text{sf}}}\right)^2\right], & \text{if } S_{\text{tss}}(s+D_v) = 0 \\ -\frac{v^2}{2D_{\text{sf}}}, & \text{if } S_{\text{tss}}(s+D_v) = 1 \end{cases} \tag{40}$$

where S_{tss} is the traffic signal status, with 1 meaning the traffic signal is red, and 0 meaning the traffic signal is green or yellow. Variable D_{sf} here indicates the distance to the traffic light when there is no preceding vehicle. In the subsequent simulations, the preview-vision distance is set to $D_v = 100$ m.

B. Deterministic Optimal Eco-Driving

Two approaches are compared in this section by tuning the cost function weight λ.

1) Time emphasized eco-driving with $\lambda = 0$, representing minimal arrival time control.
2) Fuel emphasized eco-driving with $\lambda = 1$, representing minimal fuel consumption control.

For route 1, the velocity and traveling time results of modified IDM and eco-driving control approaches are plotted in Fig. 6(a) and (b). In the modified IDM approach, the driver starts decelerating the vehicle at 12 s when it "sees" a red traffic signal in front. Due to the lack of full SPaT information, the driver is unable to incorporate future signal dynamics into its control. It switches from deceleration to acceleration as the signal turns green after 10 s, which wastes fuel. At the second traffic signal, the red light blocks the intersection. The modified IDM waits for 20 s until the light turns green. A similar situation happened at the third signalized intersection. The vehicle eventually arrives at the stop sign (the destination) at $t = 117$ s.

Considering the final arrival time for modified IDM is 117 s, we set the maximum arrival time constraint t_f in (14) to be 120 s for route 1. This ensures the optimal eco-driving approaches achieve commensurate arrival times.

In Fig. 6(b), the vehicle with eco-driving smoothly drives through the first two intersections by adjusting the velocity between 7 and 9 m/s. A deeper deceleration happens just before driving through the third signalized intersection ($s = 600$ m) to wait for a green light. After that, the vehicle velocity is restored to a higher level to ensure it arrival at the final destination within the time constraint.

The main difference between the time emphasized and fuel emphasized approaches is that the former one applies higher speeds during the 90–110-s range, which is after the last signalized intersection. In this section, the time emphasized

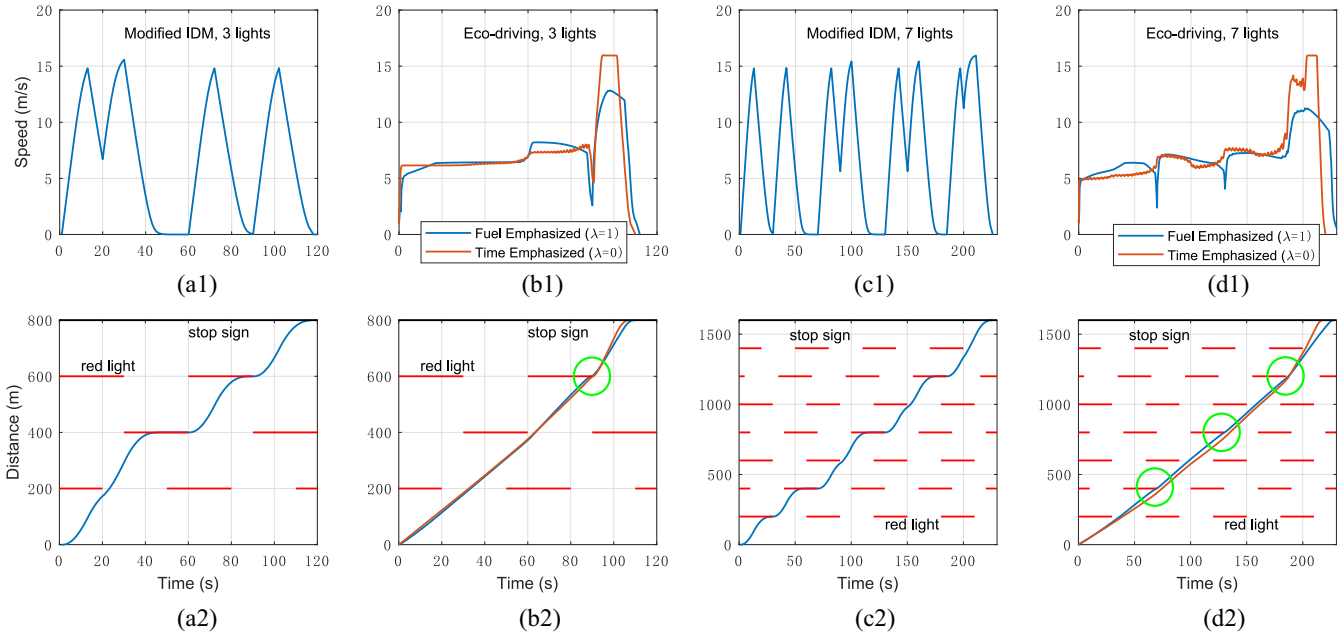

Fig. 6. Modified IDM and eco-driving results with deterministic control for routes 1 and 2. Green circles highlight driving behaviors where the vehicle passed the intersections at exact signal transition time. These behaviors could cause unexpected stopping of the vehicle, especially when there are uncertainties in traffic signal timing. The proposed data-driven robust eco-driving approach in Section IV is proposed to solve this problem.

approach uses less time to complete the driving route. The total driving time in the time emphasized case is $t = 107.6$ s, which is about 3 s shorter than the fuel emphasized case.

The vehicle velocity and traveling time results for route 2 are shown in Fig. 6(c1) and (d1), where similar phenomena are observed. The modified IDM avoids complete stops at three signalized intersections out of seven, with a final arrival time of 226 s. Here, t_f is defined as 250 s for optimal eco-driving control. As expected, the eco-driving approaches avoid aggressive accelerations of the vehicle, and cross most of the signalized intersections at lower speeds without any complete stops. The time emphasized and fuel emphasized eco-driving vehicle arrive at the destination at $t = 218.6$ and 228.5 s, respectively. The arrival time advantage is achieved by imposing higher speed during the last section. However, increasing speed at earlier sections is not helpful in reducing final arrival time, because the vehicle will be blocked by red lights. Based on the above analysis, we can draw the following remark.

Remark 1: Traffic signal timing awareness can help the vehicle avoid unnecessary deceleration or idles, without sacrificing the arrival time at the destination.

Time-dependent vehicle velocity, acceleration, engine speed, and engine torque results for route 1 are illustrated in Fig. 7. In the optimal eco-driving cases, the vehicle acceleration variation is generally milder than modified IDM. The engine speed works between 200 and 300 rad/s. The engine torque is also much smaller than modified IDM, except at time 90–100 s and time 0, when the engine generates more power to accelerate the vehicle to higher speed to guarantee the arrival time constraint is respected.

The engine BSFC results for route 1 are shown in Fig. 8. The arrival time, average BSFC, and total engine fuel consumption results for routes 1 and 2 reported in Table III.

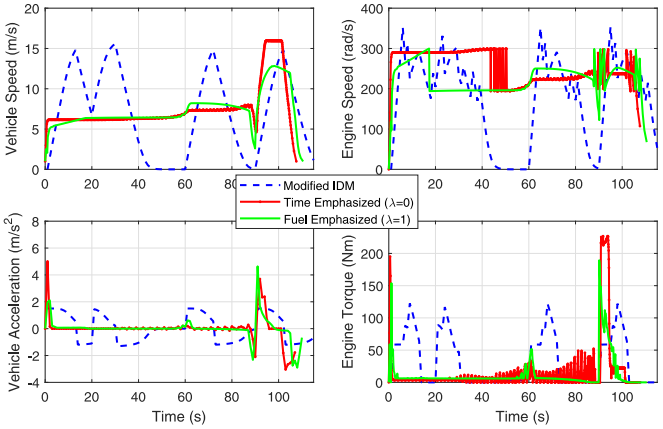

Fig. 7. Vehicle velocity, acceleration, engine speed, and torque results versus time for route 1.

TABLE III
ARRIVAL TIME, AVERAGE BSFC AND FUEL CONSUMPTION RESULTS FOR ROUTES 1 AND 2 WITH DETERMINISTIC SIGNAL TIMING

Route	Method	$t(s_f)$ (s)	$B^{\diamond}_{avg}$ (g/kWh)	Fuel (g)
800m 3 lights	Modified IDM	117	478.26	88.24
	Time emphasized	107.6	557.33	56.14
	Fuel emphasized	110.4	569.69	43.95
	Change*	-5.6%	+19.1%	-50.2%
1600m 7 lights	Modified IDM	226	477.31	172.84
	Time emphasized	218.6	562.71	101.73
	Fuel emphasized	228.5	586.53	73.90
	Change*	+1.1%	+22.9%	-57.2%

Change* means the improvement of fuel emphasized control compared with Modified IDM.
$\diamond$ B_{avg} is the average BSFC value.

The average BSFC values from the modified IDM case is less than the eco-driving approaches. This might seem counter-intuitive from an engine point of view, since lower BSFC

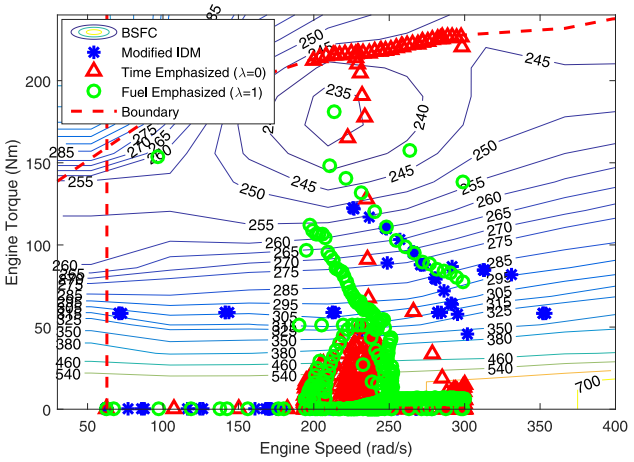

Fig. 8. Engine operating point comparison on the BSFC map for route 1.

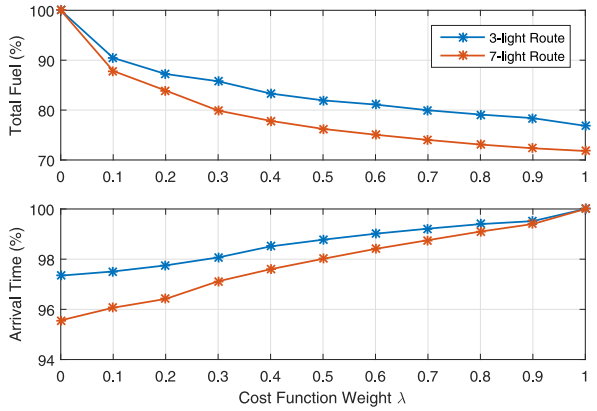

Fig. 9. Fuel comparison and arrival time performance tradeoff lines by tuning the cost function weight λ for routes 1 and 2.

values often results in better fuel economy. However, the total fuel consumption in modified IDM is much higher than the eco-driving results. The average BSFC value from time emphasized eco-driving is also lower than the fuel emphasized one, but still consumes more fuel for both test routes. The explanation is as follows: although the average engine fuel efficiency is lower, the greater wheel power requirements for modified IDM and time-emphasized eco-driving produce greater total fuel consumption. The average BSFC of fuel emphasized eco-driving is 19%–23% higher than that of modified IDM, while the overall fuel consumption is 50%–57% less. The final arrival time of the two approaches is very close, within 6% or less.

Fig. 9 shows the sensitivity of the normalized vehicle performance tradeoff lines to the parameter λ in the cost function. When $\lambda = 0$ (time emphasized control), the final arrival time is 2.5% and 4.2% lower than when $\lambda = 1$ (fuel emphasized control). However, the latter one consumes 22% and 29% less fuel in the 3-light and 7-light test routes, respectively. This result indicates that with little sacrifice on arrival time, a considerable fuel efficiency improvement can be achieved with optimal eco-driving.

Remark 2: The optimal velocity trajectories with deterministic traffic signal timing often pass through intersections exactly when the light transitions from red to green. As the switching moment approaches, SPaT uncertainties may require unexpected and sudden stopping.

The above remark can be visualized by observing the green circles in Fig. 5. This is an undesirable feature of the deterministic control formulation, namely, when the red-light duration varies away from the predicted value, a lower layer controller may unexpectedly and suddenly stop the vehicle to ensure safety. This situation endangers passenger comfort and wastes fuel. The data-driven chance-constrained robust optimal eco-driving approach is developed to address this problem, with the results presented next.

C. Data-Driven Robust Eco-Driving

Stochastic traffic light SPaT is used for the robust eco-driving validation. The deterministic part is given in Table II, and the stochastic part is given in Fig. 10.

1) Traffic Signal Timing Data: We adopt an empirical probability distribution for the traffic signal phase duration from an intersection in Montgomery, MD, USA, [35] as a case study. The traffic signal is adaptively self-controlled according to the volume of passing vehicles, which is a common design in real life. From the collected data, the stochastic part of ERD, α, follows the probability distribution shown in Fig. 11 (red curves). Similar sample distributions can also be obtained from [41] and [42].

To benchmark the eco-driving approach, we assume the distribution in Fig. 11(a) extracted from the collected data are the TRUE one. Artificially generated sample data are used for control implementation and evaluation.

This probability distribution is selected because of its interesting bimodal characteristics. The most likely red-light delays are between 1 and 2 s, possibly due to a small volume of passing vehicles. Another probability peak occurs in the range of 9.5–11.5 s of delay. We speculate that this might correspond to rush hour traffic, when the traffic flow along the perpendicular road is much greater than usual.

2) Data-Driven Chance Constraint: About 1000 sample data points are generated randomly by following the probability distribution in Fig. 11, used as the empirical data to estimate functions $\hat{\mathbb{P}}$ and $\hat{f}$. We set $\eta = 0.03$ and $d = 0.001$. The sample data histogram, calculated empirical CDF, and resultant F^{-1} estimates are all visualized in Fig. 10.

In Fig. 11(b), the equivalent $F^{-1}(1-\eta'_+)$ values calculated from χ^2, VD, and KL divergences are compared with the true $F^{-1}(1-\eta)$. We can see the $F^{-1}(1-\eta'_+)$ results are slightly greater than the true F^{-1}, with VD divergence obtaining the tightest value. This result is consistent to the perturbed risk level formulations of η'_+ in (33)–(35), which mathematically impose some conservatism due to uncertainty on the probability distribution.

Remark 3: The equivalent $F^{-1}(1-\eta'_+)$ estimates can be very close to the true $F^{-1}(1-\eta)$ with proper data samples and selections for the ϕ-divergence function and distance d.

As analyzed in Section IV-D, the probability distribution distance d has a crucial effect on the perturbed risk level η'_+.

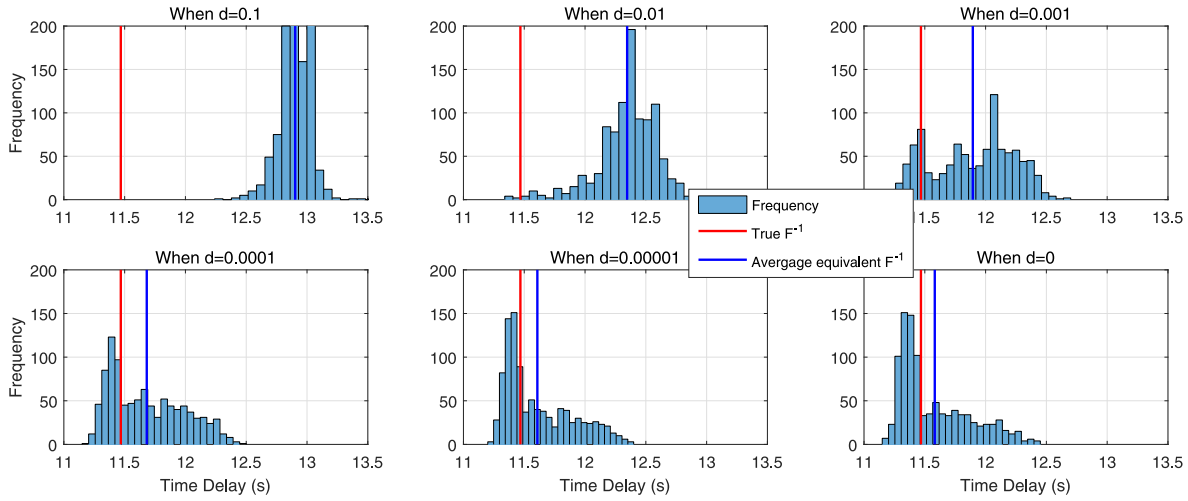

Fig. 10. Monte Carlo simulation of $F^{-1}(1-\eta'_+)$ with χ^2 divergence when sample data size $N_s = 1000$, η is set as 0.03, and d is set as 0.1, 0.01, 0.001, 0.0001, 0.00001, and 0, respectively.

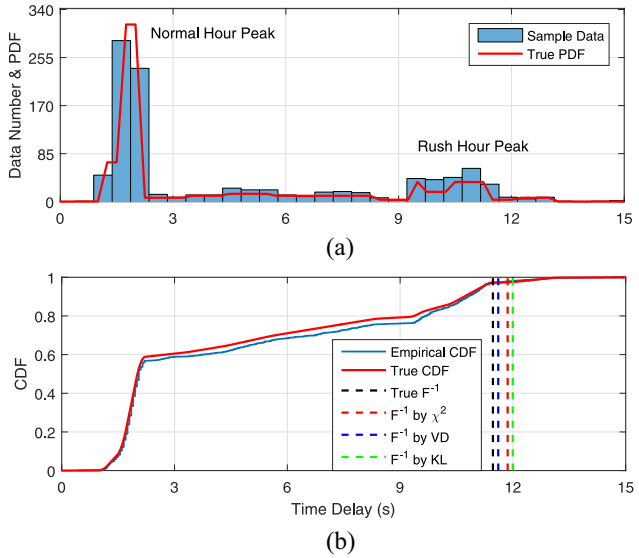

Fig. 11. Red curves are the assumed TRUE probability and CDF of α, adopted from [35]. Variable α is the stochastic time delay with respect to the nominal red-light duration. (a) Histogram of the empirical sample data randomly generated according to true PDF of α. (b) Calculated $F^{-1}(1-\eta'_+)$, compared with the true $F^{-1}(1-\eta)$, with η set as 0.03, and d set as 0.001.

A Monte Carlo simulation of $F^{-1}(1-\eta'_+)$ with χ^2 divergence when distance d varies from 0 to 0.1 is conducted. The results are illustrated in Fig. 11. If $d = 0.1$, most of the $F^{-1}(1-\eta'_+)$ values are between 12.5 and 13.5 s, whereas the true $F^{-1}(1-\eta)$ value is about 11.5 s. As we gradually reduce d, the deviation of F^{-1} decreases tremendously. When $d = 0$, the average $F^{-1}(1-\eta'_+)$ reaches its minimal value of 11.6 s, which is very close to the true F^{-1} metric 11.5 s. This result is consistent to the inverse function F^{-1} analysis with an assumed truncated Gaussian distribution on α in Fig. 5. When the sample data size N_s is greater than 500 with a small number of d, the reformulated perturbed risk level is close to the true value. Reducing d is unable to further eliminate the deviation of F^{-1}. Instead, a larger sample data size is needed.

3) Data-Driven Robust Control: In this section, the cost function weight λ is always set as 1, meaning only the fuel emphasized control is evaluated here.

Before looking at the results, we recall the hierarchical control architecture introduced in Fig. 1. The optimal eco-driving control layer is used only for velocity planning. In practice, a lower layer controller will adaptively adjust the velocity based on real-time measurements, to ensure safety. In this article, we only show the velocity planning results without the lower level controller involved.

The equivalent $F^{-1}(1-\eta'_+)$ calculated with $N_s = 1000$, $d = 0.001$, and $\eta = 0.03$, 0.1, and 0.3 are applied in the robust eco-driving approach. The vehicle trajectory and speed profile results compared to the deterministic control result for route 1 are demonstrated in Fig. 12(a) and (b). As can be seen in Fig. 12(a), the deterministic approach only considers the base red-light duration c_r^i of the traffic signal. At the third intersection, the vehicle drives through the intersection right after the base red-light duration ends. With the data-driven chance constraint used, the vehicle intentionally slows down before driving through the second and third intersections, in order to avoid high probability time delays of the red light. When $\eta = 0.03$, $F^{-1}(1-\eta'_+)$ is nearly 12 s, meaning a red-light time delay of 12 s is considered, which is the longest one in all cases. Consequently, the destination arrival time is the longest when η is set as 0.03. In Fig. 12(b), we can see that the speed profiles in the four simulations are similar during the first 60 s, before driving through the second intersection. The speed profiles diverge thereafter. To ensure the vehicle can arrive at the destination within 120 s, the vehicle speed increases to 16 m/s (road speed limit) at $t = 105$ and 108 s when $\eta = 0.03$ and 0.1, respectively.

Due to the uncertainty of the red-light durations, there is a probability that the vehicle fails to drive through the intersection with a planned speed profile. We define "Passing Probability" to evaluate the robustness, calculated by

$$\Pr(\text{passing}) = \Pr\left(c_p^i \geq c_r^i + \alpha^i\right). \tag{41}$$

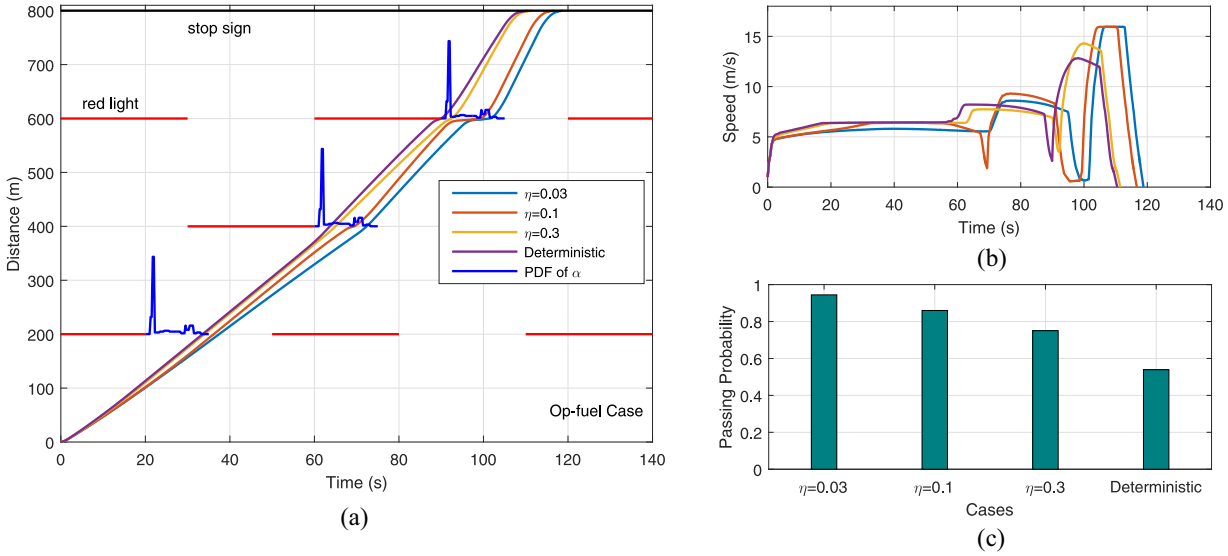

Fig. 12. (a) Vehicle traveling trajectories of fuel emphasized eco-driving control with chance reliability η set as 0.03, 0.1 and 0.3, and d set as 0.001 for route 1. The ϕ-divergence is selected to be χ^2 divergence. Sample data size $N_s = 1000$. (b) Comparison of the corresponding speed profiles. (c) Comparison of the average passing probability through the three signalized intersections.

TABLE IV
ARRIVAL TIME, FUEL, AND PASSING PROBABILITY RESULTS OF ROUTE 1

Route	Method	η	$t(s_f)$	Fuel	Pr(passing)*
800m 3 lights	Deterministic	–	110.5	44.06	53.9%
	Robust Eco-driving	0.3	111.5	45.92	75.0%
		0.1	116.7	53.29	86.0%
		0.03	118.8	52.36	94.5%

Pr(passing)* means the average passing probability.

Fig. 12(c) provides the average passing probability for the three intersections for different approaches shown in Fig. 12(a). In the deterministic approach, where red-light duration uncertainty is not considered, the average passing probability of the three signalized intersections is only 54%. With η set as 0.03, the average passing probability increases up to 94.5%. In other words, the lower control layer needs to intervene much less with robust eco-driving compared to deterministic eco-driving.

Table IV shows the arrival time, fuel consumption, and average passing probability result for the eco-driving approaches in Fig. 12. Note that significant robustness can be achieved with the small sacrifice on fuel consumption.

Remark 4: The proposed data-driven chance-constrained robust optimal eco-driving controller improves the robustness of the planned velocity trajectory. This is achieved using empirical data on the stochastic red-light delay.

The above passing probability results indicate that, even though we choose $\eta = 0.03$, there is still 5.5% probability that the vehicle requires intervention from the lower control layer to avoid a dangerous situation. This point emphasizes the relative roles of the *Motion Plan Layer* and the *Eco-Driving Control Layer* in Fig. 1, namely, even with our proposed robust eco-driving control approach, a *Motion Plan* layer is still necessary to intervene in the presence of local unexpected disturbances experienced in real time.

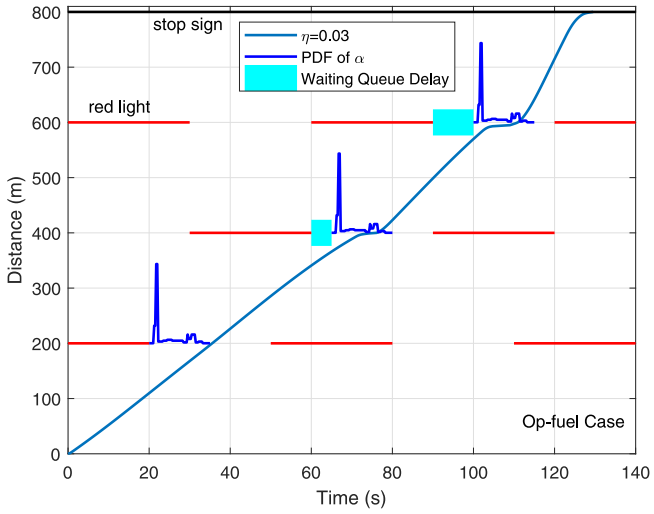

Fig. 13. Vehicle traveling trajectory of fuel emphasized eco-driving control with chance reliability η set as 0.03, with car waiting queue considered.

In Problem 4, the waiting queue time delay t_w^i is set as 0, 5, and 10 s in the three intersections of route 1, respectively. Data-driven chance-constrained optimal control is employed to search for the suboptimal velocity trajectory. The results are shown in Fig. 13. As can be seen, the ego vehicle successfully passed the intersections without conflicting with front vehicles or the red light. By comparing Figs. 12(a) and 13, the car waiting queue inevitably increased the total traveling time from 118 to 123 s.

D. Fuel Consumption and Passing Probability Evaluation

The overall fuel consumption and intersection passing probability of the proposed data-driven chance-constrained robust optimal eco-driving control is further evaluated in this section. The sample database size of α is chosen to be 50, 250, 500,

TABLE V
ARRIVAL TIME, FUEL, AND PASSING PROBABILITY RESULTS OF ROUTES 1 AND 2

Route	Method	N_s, d	$t(s_f)$	Fuel	Pr(passing)
800m 3 lights	Modified IDM	–	129	90.62	100%
	Robust Eco-driving	50, 1e-2	118.5	52.28	96.36%
		250, 1e-3	118.5	52.02	95.66%
		500, 1e-4	118.6	52.11	94.51%
		1000, 1e-5	118.7	51.94	95.98%
		2000, 0	118.6	52.09	96.19%
	Robust Eco-driving	True F^{-1}	118.8	52.36	94.45%
1600m 7 lights	Modified IDM	–	237	172.7	100%
	Robust Eco-driving	50, 1e-2	232.2	83.74	92.60%
		250, 1e-3	232.4	83.36	92.22%
		500, 1e-4	232.3	83.41	92.21%
		1000, 1e-5	232.3	83.00	92.24%
		2000, 0	232.2	82.55	91.88%
	Robust Eco-driving	True F^{-1}	232.3	78.04	89.81%

1000, and 2000, respectively. The corresponding ϕ-divergence distance d is determined based on the analysis conducted in Section IV-D and Fig. 5. The chance reliability η is always set to 0.03.

For each control approach, 100 simulations with randomly generated values of α are conducted. The resulting average arrival time (in seconds), fuel consumption (in grams), and passing probability are shown in Table V. We can see that the modified IDM consumed about 90.6 and 172.7 g of fuel on routes 1 and 2, respectively. All the robust eco-driving approaches successfully reduced the fuel consumption to under 53 and 84 g, respectively. The corresponding fuel efficiency improvements are 42% and 51%.

With proper selections of d, the data-driven chance-constrained robust optimal eco-driving control is able to achieve similar performance to the "True F^{-1}" case, where the real distribution of α is assumed to be known as a benchmark. Even when the sample database size is relatively small (for example 50), the arrival time and fuel consumption results are nearly equal to the results with large database sizes. The passing probability of modified IDM is always 100%, by construction. This is because modified IDM is, in fact, a *Motion Plan* layer control approach, and is able to observe the traffic signal SPaT in real time to adjust the vehicle speeds. We can see from Table V that the average passing probability of data-driven chance-constrained approaches is generally higher than that of true F^{-1} case. This result indicates the robustness and safety achieved by the equivalent reformulation of DCCs.

VI. CONCLUSION

A data-driven chance-constrained eco-driving control approach is proposed for velocity trajectory planning of CAVs driving through signalized intersections with uncertain signal timing. We specifically focus on endowing the optimal velocity trajectory with robustness with respect to stochastic red-light delays, thus enhancing safety and fuel economy. An equivalent reformulation of the DCCs is derived based on empirical sample data of the stochastic delay of red-light durations. The data-driven chance-constrained eco-driving controller is formulated in the spatial domain and solved by DP. Simulation results demonstrate that the fuel consumption can be significantly reduced by sacrificing less than 5% of the arrival time. The data-driven chance-constrained control approach is able to effectively improve the control robustness without requiring prior knowledge of the moments or other structural properties of the random variable distribution. We believe the proposed velocity planning and control method is a key technology enabled by the connectivity of future automobile, and can be practically applied as a driver-assistance system or the velocity planning module for CAVs.

APPENDIX
REFORMULATION OF PROBLEM 3

In (32), η' is estimated from the original risk level η and ϕ-divergence distance d

$$\eta' = 1 - \inf_{\substack{z>0, z_0+\pi z \le l_\phi, \\ \underline{m}(\phi^*) \le z_0+z \le \overline{m}(\phi^*)}} \left\{ \frac{\phi^*(z_0+z) - z_0 - \eta z + d}{\phi^*(z_0+z) - \phi^*(z_0)} \right\} \tag{42}$$

and

$$\begin{aligned} l_\phi &= \lim_{x\to+\infty} \phi(x)/x \\ \pi &= \begin{cases} -\infty, & \text{for } \mu\big([f_0 = 0]\big) = 0 \\ 0, & \text{for } \mu\big([f_0 = 0]\big) > 0 \\ 1, & \text{otherwise} \end{cases} \\ \underline{m}(\phi^*) &:= \sup\big\{m \in \mathbb{R} : \phi^* \in (-\infty, m]\big\} \\ \overline{m}(\phi^*) &:= \inf\big\{m \in \mathbb{R} : \phi^*(m) = +\infty\big\} \end{aligned} \tag{43}$$

where $\mu(\cdot)$ represents the Lebesgue measure on $\mathbb{R}$ and $[f_0 = 0] := \{\alpha \in \Omega : f_0(\alpha) = 0\}$, ϕ^* is the conjugate function of ϕ, and ϕ is a convex function defined on $\mathbb{R}^+$, with $\phi(1) = 0$ and $\phi(x) = +\infty$, for $x < 0$. Variables z and z_0 are the dual variables corresponding to the following constraints, respectively:

$$\begin{aligned} \int_\Omega \phi\left(\frac{f^*(\alpha)}{\hat{f}(\alpha)}\right)\hat{f}(\alpha)d\alpha \le d \\ \int_\Omega f(\alpha)d\alpha = 1. \end{aligned} \tag{44}$$

Specifically, for general ϕ-divergence, $l_\phi \ge \overline{m}(\phi^*)$ always stands. Without any loss of generality, the constraint $z_0 + \pi z \le l_\phi$ can be relaxed. Interested readers should consult [33, App. 2].

ACKNOWLEDGMENT

The views and opinions of authors expressed herein do not necessarily state or reflect those of the U.S. Government or any agency thereof. The authors would like to thank Prof. D. Kalathil, Prof. P. Varaiya, and Sensys Networks for substantial discussions and sharing the SPaT data.

REFERENCES

[1] A. Sciarretta, G. De Nunzio, and L. L. Ojeda, "Optimal ecodriving control: Energy-efficient driving of road vehicles as an optimal control problem," *IEEE Trans. Control Syst. Technol.*, vol. 35, no. 5, pp. 71–90, Oct. 2015.

[2] Y. J. Zhang, A. A. Malikopoulos, and C. G. Cassandras, "Optimal control and coordination of connected and automated vehicles at urban traffic intersections," in *Proc. IEEE Amer. Control Conf. (ACC)*, 2016, pp. 6227–6232.

[3] Q. Jin, G. Wu, K. Boriboonsomsin, and M. J. Barth, "Power-based optimal longitudinal control for a connected eco-driving system," *IEEE Trans. Intell. Transp. Syst.*, vol. 17, no. 10, pp. 2900–2910, Oct. 2016.

[4] N. Wan, A. Vahidi, and A. Luckow, "Optimal speed advisory for connected vehicles in arterial roads and the impact on mixed traffic," *Transp. Res. C Emerg. Technol.*, vol. 69, pp. 548–563, Aug. 2016.

[5] C. Sun, F. Sun, and S. J. Moura, "Nonlinear predictive energy management of residential buildings with photovoltaics & batteries," *J. Power Sources*, vol. 325, pp. 723–731, Sep. 2016.

[6] C. Hu, Z. Wang, Y. Qin, Y. Huang, J. Wang, and R. Wang, "Lane keeping control of autonomous vehicles with prescribed performance considering the rollover prevention and input saturation," *IEEE Trans. Intell. Transp. Syst.*, to be published.

[7] B. Paden, M. Čáp, S. Z. Yong, D. Yershov, and E. Frazzoli, "A survey of motion planning and control techniques for self-driving urban vehicles," *IEEE Trans. Intell. Veh.*, vol. 1, no. 1, pp. 33–55, Apr. 2016.

[8] A. Carvalho, S. Lefévre, G. Schildbach, J. Kong, and F. Borrelli, "Automated driving: The role of forecasts and uncertainty—A control perspective," *Eur. J. Control*, vol. 24, pp. 14–32, Jul. 2015.

[9] C. Hu *et al.*, "MME-EKF-based path-tracking control of autonomous vehicles considering input saturation," *IEEE Trans. Veh. Technol.*, vol. 68, no. 6, pp. 5246–5259, Jun. 2019.

[10] H. X. Liu and W. Ma, "A virtual vehicle probe model for time-dependent travel time estimation on signalized arterials," *Transp. Res. C Emerg. Technol.*, vol. 17, no. 1, pp. 11–26, 2009.

[11] L.-J. Zhuang, Z.-C. He, W.-J. Ye, J.-F. Chu, and L.-L. Deng, "Queue length estimation based on floating car data," *J. Transp. Syst. Eng. Inf. Technol.*, vol. 13, no. 3, pp. 78–84, 2013.

[12] E. Ozatay, Ü. Özgüner, D. P. Filev, and J. Michelini, "Analytical and numerical solutions for energy minimization of road vehicles with the existence of multiple traffic lights," in *Proc. IEEE 52nd Annu. Conf. Decis. Control (CDC)*, 2013, pp. 7137–7142.

[13] M. Muñoz-Organero and V. C. Magaña, "Validating the impact on reducing fuel consumption by using an ecodriving assistant based on traffic sign detection and optimal deceleration patterns," *IEEE Trans. Intell. Transp. Syst.*, vol. 14, no. 2, pp. 1023–1028, Jun. 2013.

[14] F. Mensing, E. Bideaux, R. Trigui, and H. Tattegrain, "Trajectory optimization for eco-driving taking into account traffic constraints," *Transp. Res. D Transp. Environ.*, vol. 18, pp. 55–61, Jan. 2013.

[15] W. Dib, A. Chasse, P. Moulin, A. Sciarretta, and G. Corde, "Optimal energy management for an electric vehicle in eco-driving applications," *Control Eng. Pract.*, vol. 29, pp. 299–307, Aug. 2014.

[16] E. Ozatay *et al.*, "Cloud-based velocity profile optimization for everyday driving: A dynamic-programming-based solution," *IEEE Trans. Intell. Transp. Syst.*, vol. 15, no. 6, pp. 2491–2505, Dec. 2014.

[17] H. Lim, W. Su, and C. C. Mi, "Distance-based ecological driving scheme using a two-stage hierarchy for long-term optimization and short-term adaptation," *IEEE Trans. Veh. Technol.*, vol. 66, no. 3, pp. 1940–1949, Mar. 2017.

[18] J. Hu, Y. Shao, Z. Sun, M. Wang, J. Bared, and P. Huang, "Integrated optimal eco-driving on rolling terrain for hybrid electric vehicle with vehicle-infrastructure communication," *Transp. Res. C Emerg. Technol.*, vol. 68, pp. 228–244, Jul. 2016.

[19] Y. Saboohi and H. Farzaneh, "Model for developing an eco-driving strategy of a passenger vehicle based on the least fuel consumption," *Appl. Energy*, vol. 86, no. 10, pp. 1925–1932, 2009.

[20] M. Kuriyama, S. Yamamoto, and M. Miyatake, "Theoretical study on eco-driving technique for an electric vehicle with dynamic programming," in *Proc. IEEE Int. Conf. Elect. Mach. Syst. (ICEMS)*, 2010, pp. 2026–2030.

[21] B. HomChaudhuri, A. Vahidi, and P. Pisu, "A fuel economic model predictive control strategy for a group of connected vehicles in urban roads," in *Proc. IEEE Amer. Control Conf. (ACC)*, 2015, pp. 2741–2746.

[22] M. A. S. Kamal, M. Mukai, J. Murata, and T. Kawabe, "On board eco-driving system for varying road-traffic environments using model predictive control," in *Proc. IEEE Int. Conf. Control Appl. (CCA)*, 2010, pp. 1636–1641.

[23] M. Li, K. Boriboonsomsin, G. Wu, W.-B. Zhang, and M. Barth, "Traffic energy and emission reductions at signalized intersections: A study of the benefits of advanced driver information," *Int. J. Intell. Transp. Syst. Res.*, vol. 7, no. 1, pp. 49–58, 2009.

[24] S. E. Li, S. Xu, X. Huang, B. Cheng, and H. Peng, "Eco-departure of connected vehicles with V2X communication at signalized intersections," *IEEE Trans. Veh. Technol.*, vol. 64, no. 12, pp. 5439–5449, Dec. 2015.

[25] V. A. Butakov and P. Ioannou, "Personalized driver assistance for signalized intersections using V2I communication," *IEEE Trans. Intell. Transp. Syst.*, vol. 17, no. 7, pp. 1910–1919, Jul. 2016.

[26] G. De Nunzio, C. C. Wit, P. Moulin, and D. Di Domenico, "Eco-driving in urban traffic networks using traffic signals information," *Int. J. Robust Nonlin. Control*, vol. 26, no. 6, pp. 1307–1324, 2016.

[27] X. He, H. X. Liu, and X. Liu, "Optimal vehicle speed trajectory on a signalized arterial with consideration of queue," *Transp. Res. C Emerg. Technol.*, vol. 61, pp. 106–120, Dec. 2015.

[28] B. HomChaudhuri, A. Vahidi, and P. Pisu, "Fast model predictive control-based fuel efficient control strategy for a group of connected vehicles in urban road conditions," *IEEE Trans. Control Syst. Technol.*, vol. 25, no. 2, pp. 760–767, Mar. 2017.

[29] H. Yang, H. Rakha, and M. V. Ala, "Eco-cooperative adaptive cruise control at signalized intersections considering queue effects," *IEEE Trans. Intell. Transp. Syst.*, vol. 18, no. 6, pp. 1575–1585, Jun. 2017.

[30] X. Huang and H. Peng, "Speed trajectory planning at signalized intersections using sequential convex optimization," in *Proc. IEEE Amer. Control Conf. (ACC)*, 2017, pp. 2992–2997.

[31] G. Mahler and A. Vahidi, "An optimal velocity-planning scheme for vehicle energy efficiency through probabilistic prediction of traffic-signal timing," *IEEE Trans. Intell. Transp. Syst.*, vol. 15, no. 6, pp. 2516–2523, Dec. 2014.

[32] C. Sun, X. Shen, and S. Moura, "Robust optimal eco-driving control with uncertain traffic signal timing," in *Proc. IEEE Amer. Control Conf. (ACC)*, 2018, pp. 5548–5553.

[33] R. Jiang and Y. Guan, "Data-driven chance constrained stochastic program," *Math. Program.*, vol. 158, nos. 1–2, pp. 291–327, 2016.

[34] S. Halbach, P. Sharer, S. Pagerit, A. P. Rousseau, and C. Folkerts, "Model architecture, methods, and interfaces for efficient math-based design and simulation of automotive control systems," Tech. Paper 2010-01-0241, SAE, Warrendale, PA, USA.

[35] S. Ibrahim, D. Kalathil, R. O. Sanchez, and P. Varaiya, "Estimating phase duration for SPaT messages," *IEEE Trans. Intell. Transp. Syst.*, vol. 20, no. 7, pp. 2668–2676, Jul. 2019.

[36] O. Sundström, D. Ambühl, and L. Guzzella, "On implementation of dynamic programming for optimal control problems with final state constraints," *Oil Gas Sci. Technol. Revue de la Institut Français du Pétrole*, vol. 65, no. 1, pp. 91–102, 2010.

[37] A. Sciarretta and L. Guzzella, "Control of hybrid electric vehicles," *IEEE Trans. Control Syst. Technol.*, vol. 27, no. 2, pp. 60–70, Apr. 2007.

[38] C. Sun, S. J. Moura, X. Hu, J. K. Hedrick, and F. Sun, "Dynamic traffic feedback data enabled energy management in plug-in hybrid electric vehicles," *IEEE Trans. Control Syst. Technol.*, vol. 23, no. 3, pp. 1075–1086, May 2015.

[39] A. Rousseau *et al.*, "Electric drive vehicle development and evaluation using system simulation," *J. Soc. Instrum. Control Eng.*, vol. 53, no. 4, pp. 314–321, 2014.

[40] A. Kesting, M. Treiber, and D. Helbing, "Enhanced intelligent driver model to access the impact of driving strategies on traffic capacity," *Philos. Trans. Roy. Soc. London A Math. Phys. Eng. Sci.*, vol. 368, no. 1928, pp. 4585–4605, 2010.

[41] S. Axer and B. Friedrich, "Estimating signal phase and timing for traffic actuated intersections based on low frequency floating car data," in *Proc. IEEE 19th Int. Conf. Intell. Transp. Syst. (ITSC)*, 2016, pp. 2059–2064.

[42] S. A. Fayazi and A. Vahidi, "Crowdsourcing phase and timing of pretimed traffic signals in the presence of queues: Algorithms and back-end system architecture," *IEEE Trans. Intell. Transp. Syst.*, vol. 17, no. 3, pp. 870–881, Mar. 2016.

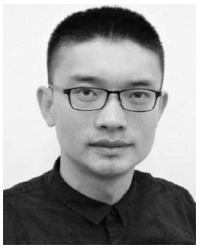

Chao Sun (Member, IEEE) received the B.S. degree in mechanical engineering from Beihang University, Beijing, China, in 2010, and the Ph.D. degree in mechanical engineering from the Beijing Institute of Technology, Beijing, in 2016.

He was a Postdoctoral Researcher with the Energy, Controls, and Applications Laboratory, University of California at Berkeley, Berkeley, CA, USA. He is currently an Associate Professor with the Beijing Institute of Technology, studying on model predictive control and data-driven forecasting with applications to automated and connected vehicles and hybrid electric vehicles.

Jacopo Guanetti (Member, IEEE) was born in Varese, Italy, in 1987. He received the B.Sc. and M.Sc. degrees in automation engineering and the Ph.D. degree in systems and control engineering from the Politecnico di Milano, Milan, Italy, in 2009, 2012, and 2015, respectively.

In 2012, he was a Visiting Scholar with the Center for Automotive Research, Ohio State University, Columbus, OH, USA. He is currently a Postdoctoral Researcher with the University of California at Berkeley, Berkeley, CA, USA. His research interests include optimal and predictive control, with applications to the control of vehicle dynamics, connected and automated vehicles and hybrid electric powertrains.

Francesco Borrelli (Fellow, IEEE) received the Laurea degree in computer science engineering from the University of Naples "Federico II," Naples, Italy, in 1998, and the Ph.D. degree from Automatic Control Laboratory, ETH-Zurich, Zürich, Switzerland, in 2002.

He is currently a Professor with the Department of Mechanical Engineering, University of California at Berkeley (UC Berkeley), Berkeley, CA, USA. He was the Founder and the CTO of BrightBox Technologies Inc., Berkeley, a company focused on cloud-computing optimization for autonomous systems. He is the Co-Director of the Hyundai Center of Excellence in Integrated Vehicle Safety Systems and Control, UC Berkeley. He is the CTO of software of NEXTracker, Inc., Fremont, CA, USA, the world leader company in photovoltaic trackers. He has authored the book *Predictive Control* (Cambridge University Press). His research interests are in the area of model predictive control and its application to automated driving and energy systems.

Prof. Borrelli is the winner of the 2009 NSF CAREER Award and the 2012 IEEE Control System Technology Award. In 2017, he was awarded the Industrial Achievement Award by the International Federation of Automatic Control Council. Since 2004, he has served as a consultant for major international corporations.

Scott J. Moura (Member, IEEE) received the B.S. degree in mechanical engineering from the University of California at Berkeley, Berkeley, CA, USA, in 2006, and the M.S. and Ph.D. degrees in mechanical engineering from the University of Michigan at Ann Arbor, Ann Arbor, MI, USA, in 2008 and 2011, respectively.

He is currently an Associate Professor and the Director of civil and environmental engineering with the Energy, Controls, and Applications Laboratory, University of California at Berkeley, where he is an Assistant Professor with the Smart Grid and Renewable Energy Laboratory, Tsinghua–Berkeley Shenzhen Institute, Berkeley. From 2011 to 2013, he was a Postdoctoral Fellow with the Cymer Center for Control Systems and Dynamics, University of California at San Diego, San Diego, CA, USA. In 2013, he was a Visiting Researcher with the Centre Automatique et Systèms, MINES ParisTech, Paris, France. His research interests include optimal and adaptive control, partial differential equation control, batteries, electric vehicles, and energy storage.

Dr. Moura is a recipient of the National Science Foundation Graduate Research Fellowship, the UC Presidential Postdoctoral Fellowship, the O. Hugo Shuck Best Paper Award, the ACC Best Student Paper Award (as advisor), the ACC and ASME Dynamic Systems and Control Conference Best Student Paper Finalist (as student), the Hellman Fellows Fund, University of Michigan Distinguished ProQuest Dissertation Honorable Mention, University of Michigan Rackham Merit Fellowship, College of Engineering Distinguished Leadership Award.